CORA Cork Open Research Archive
Cartlann Taighde Oscailte Chorcaí

Title	TiO2 nanocluster modified-rutile TiO2 photocatalyst: a first principles investigation
Authors	Iwaszuk, Anna;Mulheran, Paul A.;Nolan, Michael
Publication date	2013-01-02
Original Citation	Iwaszuk, A., Mulheran, P. A. and Nolan, M. (2013) 'TiO2 nanocluster modified-rutile TiO2 photocatalyst: a first principles investigation', Journal of Materials Chemistry A, 1(7), pp. 2515-2525. doi: 10.1039/c2ta01582j
Type of publication	Article (peer-reviewed)
Link to publisher's version	10.1039/c2ta01582j
Rights	© The Royal Society of Chemistry 2013. This is the Accepted Manuscript version of a published work that appeared in final form in Journal of Materials Chemistry A. To access the final published version of record, see http://pubs.rsc.org/en/content/articlepdf/2013/ta/c2ta01582j
Download date	2026-11-16 09:00:50
Item downloaded from	https://hdl.handle.net/10468/1594



UCC
University College Cork, Ireland
Coláiste na hOllscoile Corcaigh

Journal Name

Dynamic Article Links ►

Cite this: DOI: 10.1039/c0xx00000x

www.rsc.org/xxxxxx

ARTICLE TYPE

TiO_2 Nanocluster Modified-Rutile TiO_2 Photocatalyst: a First Principles Investigation

Anna Iwaszuk[a], P. A. Mulheran[b] and Michael Nolan[a]

Received (in XXX, XXX) Xth XXXXXXXXX 200X, Accepted Xth XXXXXXXXX 200X

First published on the web Xth XXXXXXXXX 200X

DOI: 10.1039/

Abstract Titanium dioxide is an important photocatalytic material with much activity in modifying it to achieve visible light absorption. Recently, studies targeting the modification of TiO_2 with metal oxide nano clusters have investigated heterostructures which show potential as new TiO_2-based photocatalytic materials with visible light absorption and improved photocatalytic activity. Obtaining detailed insights into the influence of surface modification on the photocatalytic properties of TiO_2 will further the possibilities for using this approach to develop new photocatalysts. In this paper, we present the results of density functional theory (DFT) simulations of the TiO_2 rutile (110) surface modified with TiO_2 nanoclusters ($(TiO_2)_n$: Ti_5O_{10}, Ti_6O_{12}, Ti_8O_{16}, $Ti_{16}O_{32}$, $Ti_{30}O_{60}$), with diameters up to 1.5 nm, which is a cluster size achievable in experiments. The clusters adsorb strongly at the surface giving adsorption energies from -2.7 eV to -6.7 eV. The resulting structures show a large number of new Ti-O bonds created between the cluster and the surface, so that the new bonds enhance the stability. The electronic density of states (EDOS) shows that the valence band edge is shifted upwards, due to new nanocluster derived states in this region, while the conduction band is unchanged and composed of the Ti 3d states from the surface. This reduces the band gap over bare TiO_2, potentially shifting light absorption into the visible region. The valence and conduction band composition of these heterostructures will favour spatial separation of electrons and holes after light excitation, thus giving improved photocatalytic properties in these novel structures.

1. Introduction

Photocatalytic technologies have great potential as low cost, environmentally friendly catalysts for environmental depollution by destruction of organic pollutants[1,2], removal of bacteria such as MRSA[3,4] and the interesting possibility of solar hydrogen production from water splitting[5-7]. A leading material is titanium (IV) dioxide, TiO_2, which is cheap, readily available and non-toxic. Since the band gap of the rutile and anatase forms of TiO_2 lies in the UV region (typically in the range of 3 eV to 3.2 eV) a major activity in delivering widespread photocatalytic technologies is to shift the band gap in order to have a material that will be active in the visible region of the solar spectrum, thus using a larger fraction of the available solar energy than that available in the UV[8,9].

Until recently, most efforts in modifying TiO_2 to enhance visible light absorption have focused on substitutional cation or anion doping at Ti or O sites [10-18] to achieve a band gap reduction. Recent work has treated co-doping with compensating cation-anion pairs[19-21]. The aim of narrowing the band gap is an important activity, however, it has to be emphasised that there are other issues like stability, solubility and reproducibility in doping TiO_2, as well as the impact of doping on electron-hole recombination. There are other semiconductors with photoactive properties, including ZnO, $SrTiO_3$, CeO_2, WO_3, Fe_2O_3, GaN, Bi_2S_3, CdS, and ZnS[22].

Recent results indicate that an alternative approach, namely fabricating heterostructures of two different metal oxides is a promising avenue for inducing visible light absorption and improving photocatalytic activity[23-36], in particular for photodegradation of molecules[29-31]. Of course, the mixed rutile-anatase heterostructure, also known as Degussa P25, is a well known photocatalyst with better photocatalytic properties than pure rutile or anatase[37-39]. This is attributed to the presence of the interface between rutile and anatase[37-41] although there is still some debate as to the origin of the photocatalytic activity of the rutile-anatase heterostructures. ZnO-TiO_2 heterostructures have also been studied in photocatalysis[40,41], and displays a charge separation as a result of heterostructure formation While the idea of TiO_2 based photocatalytically heterostructures is of course not new, there

has been an increased activity in alternative materials and in using nanostructures.

A heterostructure of doped rutile Sn:TiO_2 and doped anatase N:TiO_2 was synthesised[23] and showed improved photocatalytic activity in the visible and UV regions, when compared to rutile TiO_2-Sn or anatase TiO_2-N, due to heterojunction formation in the interface and an increase in the amount of photogenerated charge carriers[23]. Recent studies have revealed that oxide heterostructures such as BiOBr-$ZnFe_2O_4$[24], AgI-BiO[25], $BiVO_4$-WO_3[26], $Bi_4Ti_3O_{12}$-TiO_2[27] and SnO_x-$ZnGa_2O_4$[28] and their interfaces feature enhanced photocatalytic activities compared to the pure oxides. These heterostructures have a reduced band gap which shifts the photoactivity into the visible region, while promoting electron and hole separation.

Recently, novel heterostructures formed from surface modification of TiO_2 with metal oxide nanoclusters have been investigated by Libera et al.[29] and Tada et al.[30] for FeO_x modified TiO_2. Libera at al deposited Fe_2O_3 nanoclusters by atomic layer deposition (ALD) on TiO_2 and found visible light absorption and efficient photocatalytic degradation of methylene blue[29]. (FeO_x)-modified TiO_2 was synthesised using the chemisorption-calcination-cycle (CCC) by Tada and co-workers, depositing highly dispersed metal oxide nanoclusters on the TiO_2 surface at a molecular scale[30]. The (FeO_x)/TiO_2 system showed greatly improved visible light activity and also good UV-light activity for degradation of naphthol (a dye precursor) which arose from band gap narrowing due to the presence of the (FeO_x) clusters shifting the top of the TiO_2 valence band[30]. Moreover photoluminescence (PL) spectroscopy indicated a decrease in electron-hole recombination[30].

In subsequent work, Tada and co-workers have studied NiO[31] and SnO_2[32,33] modified TiO_2 for their ability to enhance visible or UV photocatalytic activity of TiO_2; with NiO-modified TiO_2 showing similar visible light absorption and enhanced photocatalytic activity to FeO_x modified TiO_2. Interestingly, while SnO_2-modified anatase TiO_2 showed only UV activity[32], SnO_2 modified rutile displayed some visible light activity and improved UV activity[33]. In all cases, the activity was reported for dye degradation, which is important for environmental applications. The question of the potential utility of these structures for photocatalytic water splitting has not been addressed to date and remains an interesting avenue of exploration.

In understanding the findings of these experimental studies and in particular, the effect of surface modification on the light absorption properties and on the reactivity, density functional theory (DFT) simulations of TiO_2 modified with small metal oxide clusters have confirmed the origin of the band gap reduction in FeO_x modified rutile TiO_2[34] as well as the origin of the enhanced UV or visible light activity of SnO_2-modified anatase[32] or rutile[33] TiO_2. In addition, we previously showed that sub-nm diameter $(TiO_2)_n$ clusters, with n=2-4, adsorbed on the rutile TiO_2 (110) surface can lead to a reduced band gap compared to pure rutile TiO_2, which should enhance the photocatalytic activity in these heterostructures[35], although a focus in that paper was on the reactivity of these structures. DFT simulations have also shown that modifying the rutile (110) surface with small transition metal oxide nanoclusters, e.g. Cr_2O_3, Mo_2O_4, could also lead to a band gap reduction[36]. One point to note is that these DFT studies have all considered metal oxide clusters with diameters smaller than 1 nm. Such clusters show size dependent properties, such as energy gaps. Transmission electron microscopy investigations of CCC synthesised structures have indicated that the FeO_x and NiO particles adsorbed by the CCC technique have diameters around 1 - 2 nm[30,31] and that the oxide nanoclusters supported on rutile or anatase do not aggregate into larger clusters or films.

In this paper we investigate with DFT heterostructures of the rutile (110) surface modified with TiO_2 nanoclusters with diameters up to 1.5 nm as new visible light active photocatalytic materials. This study therefore includes nanoclusters at the dimensions found in experiment, facilitating a more direct comparison with experiment. We generate representative cluster-surface structures, determined from initial interatomic potential simulations of adsorbed $(TiO_2)_n$ clusters, where n = 5, 6, 8, 16, 30 on the rutile TiO_2 (110) surface and present the electronic properties of the heterostructures. We find that all clusters adsorb strongly at the surface creating new interfacial Ti-O bonds between the cluster and the surface. Analysis of the electronic structure and optical absorption spectrum indicates that a narrowing of the band gap by deposition of TiO_2 nanoclusters is possible, with the precise extent of narrowing depending on the size of the TiO_2 nanocluster, while the energy band alignments indicate that charge carrier separation upon excitation will be enhanced. This work demonstrates that surface modified TiO_2 with nanoclusters is a potentially useful approach for engineering the photocatalytic properties of TiO_2.

2. Methodology

For modelling TiO_2 rutile (110) we use a three dimensional periodic slab model in the VASP code[42]. The valence electrons are described by a plane wave basis set and the cut-off for the kinetic energy is 396 eV. The core-valence interaction is described with the projector augmented wave approach[43] and there are 4 valence electrons for Ti and 6 valence electrons for O. In a previous paper[44], we compared the description of the properties of TiO_2 with small and large core Ti PAW potentials and found no significant differences between the two potentials. The exchange-correlation functional is the approximation of Perdew-Wang (PW91)[45]. The Monkhorst-Pack scheme is used for k-point sampling with a (2x2x1) sampling grid, while the largest structures use Γ-point sampling. The (110) surface is terminated by two-fold coordinated bridging oxygen atoms and the next sublayer consists of 6-fold and 5-fold coordinated Ti atoms. In order to ensure that the clusters are isolated we employed a (2x4) surface supercell, while a (4x8) surface supercell is used for adsorption of $Ti_{16}O_{32}$ and $Ti_{30}O_{60}$ clusters. The cluster supercells have the same parameters as the corresponding supercell for the cluster-surface heterostructures.

For the calculations we use DFT and DFT corrected for on-

site Coulomb interactions (DFT+U)[46,47] where we have applied U = 4.5 eV on the Ti 3d states[35,48]. The need to introduce the U parameter in order to describe properly the electronic states of d shells, such as reduced Ti^{3+}, is well known[49,50]. While we do not have Ti^{3+} states directly formed in the present heterostructures, the possibility of Ti^{3+} formation in subsequent reactions at the heterostructures makes the use of DFT+U necessary[35], as does the choice of U = 4.5 eV, which is suitable for describing oxygen vacancies in TiO_2 surfaces[49]. We also present some results for the DFT simulations for selected structures to show the insensitivity of our key results to the choice of DFT or DFT+U. While both DFT and DFT+U underestimate the band gap and the energy gap depends on the precise DFT+U set up, we are aware of this issue and hence the change in band gap, which is reliable, is our primary focus. DFT shows reasonable reliability in qualitatively determining energy gap changes upon doping, despite the error in the energy gap, with refs. 11, 19, 21, 51, 52 showing that changes in the energy gap of TiO_2 with doping are reliable.

To investigate the effect of modifying rutile TiO_2 with the nanoclusters, we compute the optical (Tauc) gap of these structures. The optical gap is obtained by plotting the absorption coefficient against photon energy and extrapolating the linear part of the plot. To do this, we use the postprocessing routines of Furthmueller[53] to calculate the real and imaginary parts of the dielectric function, ε_1 and ε_2. From this the extinction coefficient, κ, is obtained:

$$\kappa = 1/\sqrt{2}\,(-\varepsilon_1 + (\varepsilon_1^2 + \varepsilon_2^2)) \qquad (2)$$

and from κ, we compute the absorption coefficient:

$$\alpha = 2\kappa\pi/\lambda \qquad (1)$$

Where λ is the free space wavelength of light. Extrapolating the linear part of the plot of absorption coefficient against photon energy gives the optical gap.

While DFT calculations are excellent at providing details on the electronic properties of the type of heterostructures studied in this paper, screening many different adsorption structures becomes unfeasible for structures of the size considered herein. Therefore, a realistic atomistic potential based model can be used to determine favourable adsorption structures for further refinement with DFT. There is much interest in using the charge equilibration (QEq) scheme of Rappé and Goddard[54,55] for TiO_2 structures, in which the electronegativity of the ions is used to adjust the charge distribution in an adaptive manner. In our recent work, the application of this approach to TiO_2 has been demonstrated via the QEq methodology[56] which allows charge transfer between ions to minimise the electrostatic energy Ees, whilst including contributions from the charging energies for each ion which takes a parabolic form:

$$E_{es} = \sum_i (E_i^0 + \chi_i^0 q_i + J_i^0 q_i^2) + \tfrac{1}{2}\sum_{i \neq j} J_{ij} q_i q_j \qquad (1)$$

where χ_i^0 and J_i^0 are related to the electronegativity and hardness of the ions, respectively. J_{ij} is the shielded Coulomb interaction between ions. The shielding is estimated by the overlap of *s*-type Slater orbitals. For any ionic configuration, the charge q_i on the Ti ions is adjusted to minimise equation (1) under the constraint of conserved total charge

$$\sum_i q_i = 0$$

without moving the ionic positions. Once equilibration has been achieved, the forces on the ions are used to move them in a standard minimisation or dynamics algorithm. The atomistic model includes short-range potentials to represent the covalent bonding which is significant for TiO_2. A criticism of the QEq approach is that it can underestimate ionic contributions to the energetics and elastic properties of TiO_2 and that the electrostatics actually play no role in the description of TiO_2, e.g. in the Swamy-Gale model[57,58]. Hallil *et al* have corrected the deficiency in the QEq approach by changing the functional form of the covalent interactions, by using a pair-functional form to describe Ti-O covalent bonds[59,60]. This provides a more responsive description of the short-range bonding terms, and allows the variable-charge advantage of the QEq scheme to be retained[60]. We have found that the behaviour of oxygen within the Hallil model indicates that the energetics of the QEq component underplay the costs of moving the charge both to and from the oxygen and in our calculations we keep the charge on all oxygens fixed to their bulk value of $1.26e^-$, with only the Ti ions able to transfer charge between themselves using the original charging self-energies[56]. This modification better reproduces the very small changes seen in oxygen charge found with DFT+U; further details can be found in refs.[56,59,60].

In determining the structures of the free TiO_2 clusters, we have used the QEq potential in conjunction with a Monte Carlo search approach to compute the lowest energy structural isomers of a given TiO_2 composition. Minimised TiO_2 clusters were created using the parallel tempering technique[61] with the charge equilibration (QEq) potential[59,60]. The initial positions of the ions in the cluster were randomly chosen, followed by Monte Carlo simulation in an ordered series of replicas 1,2,…N. Each replica had a different temperature; replica 1 was at 300K, and the temperature of replica N (7000K) was chosen so that the cluster is just able to dissociate with the potential field employed. At regular intervals during the simulation, the energies of the configurations in neighbouring replicas were compared, and the replica configurations swapped according to Boltzmann probabilities. The frequency of the comparisons, and the value of N, is chosen to allow a reasonable rate of exchange (about 20%) amongst the replicas. We found N=7 worked well. The QEq potential allows for the transfer of charge between the Ti ions. In our simulation, we treated the movement of charge (preserving overall charge conservation) as an alternative Monte Carlo step to the positional changes of the ions. At the end of the tempering simulation, the replica structures were minimised so that charge equilibration is established and the configuration is at its energy minimum. The lowest energy structure of each TiO_2 nanocluster found in the low-temperature replicas were then input into VASP and relaxed with DFT+U to provide the final free cluster structures, which were then adsorbed onto the rutile (110) surface in different adsorption configurations.

QEq relaxations were further used to determine the energies of a number of cluster-surface structures for each TiO_2 cluster, with the adsorption structures ranked by energy. Since the QEq approach gives a good description of the structure in TiO_2 compared with DFT[59,60] and DFT+U[56], the most stable cluster-surface heterostructures found with QEq are a reliable starting point for subsequent relaxation with DFT+U (with DFT for selected comparisons) and the resulting adsorption energy is computed from:

$E^{ads} = E((TiO_2)_n\text{-}TiO_2) - \{ E((TiO_2)_n) + E(TiO_2) \}$ (2),

where $E((TiO_2)_n\text{-}TiO_2)$ is the total energy of the $(TiO_2)_n$ cluster supported on the rutile (110) surface, $E((TiO_2)_n)$ and $E(TiO_2)$ are the total energies of the free cluster and the bare surface respectively. A negative adsorption energy signifies that cluster adsorption is stable relative to the free cluster and bare surface.

3. Results

Figure 1 presents the atomic structure of the pure TiO_2 (110) surface and the free TiO_2 clusters (which are DFT+U relaxed structures from the initial Monte-Carlo and QEq generated structures) namely: Ti_5O_{10}, Ti_6O_{12}, Ti_8O_{16}, $Ti_{16}O_{32}$, $Ti_{30}O_{60}$. Consistent with earlier studies[62-65] the TiO_2 nanoclusters show smaller Ti and O coordination numbers, e.g. 4 and 5 coordinated Ti compared to 6 coordinated bulk Ti and 1, 2 and 3 coordinated oxygen compared to 3 coordination in bulk rutile. The clusters we consider do not show any faceting into surfaces, as is seen for CeO_2 clusters of similar size[66] However, SiO_2 clusters also show non-bulk like structures even up to 2 nm diameter, which is typical for materials with a covalent character, while ionic materials tend to show bulk-like structures at smaller sizes.

Each cluster presents terminal oxygen atoms that are coordinated to one Ti - for Ti_5O_{10} there are two terminal oxygen atoms while the biggest cluster $Ti_{30}O_{60}$, has eight terminal oxygen atoms. The Ti-O distances in the clusters are usually shorter than in the bulk and for terminal oxygen atoms the Ti-O distances are particularly short, at 1.68 Å while remaining Ti-O bonds are in the range of 1.7Å - 2.1Å. The TiO_2 clusters considered are stoichiometric because for these clusters we compute that the formation of an oxygen vacancy, to give a reduced nanocluster, has an energy cost.

Finally, for reference, we consider the computed Bader[67] charges on Ti and O in the free clusters. Ti atoms in the free clusters are all in the Ti^{4+} oxidation state, with computed Bader charges of 1.38 – 1.45 electrons (net charge of +2.62 to +2.55 electrons), typical for oxidised Ti^{4+}. With oxygen having three different coordination numbers, we obtain three sets of Bader charges: terminal oxygens have the least negative charge of 7.14 electrons (net charge of -1.14 electrons), 2-fold coordinated oxygen have negative charges around 7.30 electrons (net -1.30 electrons) and 3-fold coordinated oxygen have computed charges around 7.40 electrons (net -1.40 electrons). By comparison, in bulk rutile, the computed Ti and O charges are 1.38 (net +2.62 electrons) and 7.31 electrons (net -1.31 electrons) and a Ti^{3+} species (arising from an oxygen vacancy) has a computed Bader charge of +1.70 electrons, giving a net charge of +2.30 electrons. The variation in the Bader charge on the cluster oxygen, +/- 0.12e, is similar in magnitude to that found in our study of adatoms and interstitials in the rutile (110) selvedge[56], where our modified QEq methodology was derived.

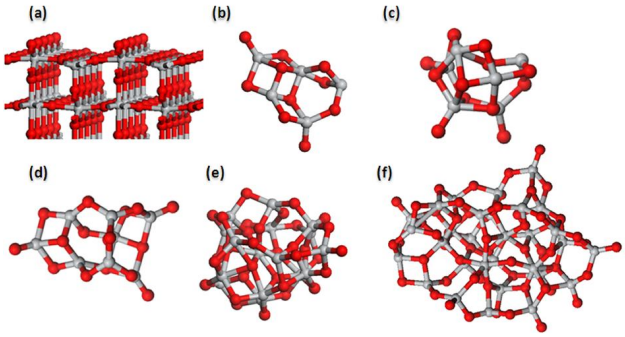


Fig1 Atomic structure of (a) TiO_2 rutile (110) surface, (b) Ti_5O_{10}, (c) Ti_6O_{12}, (d) Ti_8O_{16}, (e) $Ti_{16}O_{32}$, (f) $Ti_{30}O_{60}$ clusters; the nanocluster structures shown are relaxed with the DFT+U setup described in section 2. The grey spheres are Ti atoms and the red spheres are O atoms; this colour scheme is used in the remainder of the figures.

Figure 2 presents the atomic structure and adsorption energies of four configurations of Ti_5O_{10} deposited on TiO_2 (110) surface. We use this cluster-surface heterostructure as an example to discuss the properties of different adsorption configurations of the same cluster on the rutile (110) surface. For the other cluster-surface structures, we show only the most stable structures as measured by the adsorption energy in figure 3, while other, less stable, configurations of these cluster-surface structures are shown in the supporting information (figure S1, S2).

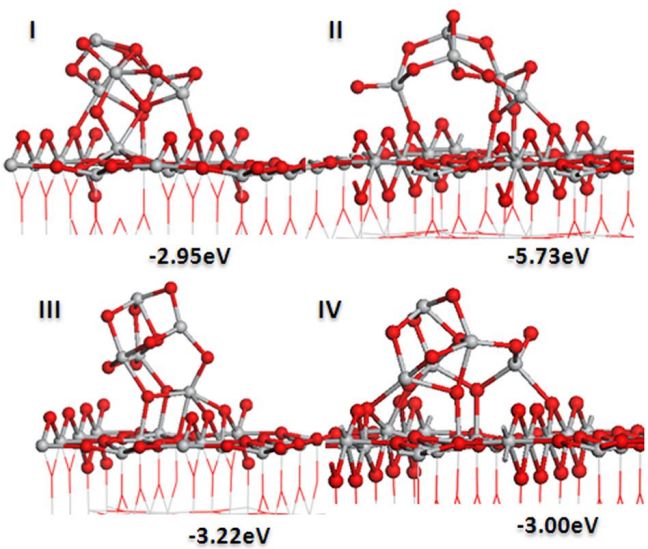


Fig.2 Relaxed adsorption structures with adsorption energies (in eV) for different configurations of the Ti_5O_{10} cluster on the TiO_2 rutile (110) surface. The Roman numerals shows the numbering of cluster configurations.

The computed adsorption energies for the four adsorption configurations of Ti_5O_{10} show a strong interaction between the cluster and the surface, being in the range from -2.95 eV to -5.70 eV. The most stable Ti_5O_{10}, Ti_6O_{12}, Ti_8O_{16}, $Ti_{16}O_{32}$ and $Ti_{30}O_{60}$ clusters adsorbed on the TiO_2 rutile (110) surface show adsorption energies in the range from -2.72 eV for Ti_6O_{12} cluster to -6.71 eV for the $Ti_{30}O_{60}$ cluster, displaying both strong anchoring of the nanocluster at the rutile surface and a distinct cluster size effect.

When nanoclusters adsorb at the TiO_2 surface, it is important to consider the possibility of cluster aggregation that could take place during, e.g. sintering treatments. To examine this in a simple fashion, we consider the energies involved in the stability of a supported TiO_2 nanocluster that is aggregated from smaller nanoclusters in comparison to the situation where these clusters are isolated. For example, we can examine the energies of a supported Ti_6O_{12} cluster compared to the energy of two Ti_3O_6 clusters. The energies computed for a selection of possible cluster aggregation schemes are shown in the supporting information; we note that in examining the energetics for modified rutile (110), we can only compare those structures with the same rutile (110) surface model, limiting our analysis to the structures for which energies are given in the supporting information.

These results show the following. Gas phase nanoclusters display a preference to aggregate to form larger nanoclusters. However when the nanoclusters are anchored at the rutile (110) surface, we find the opposite, namely that cluster aggregation is energetically disfavoured, so that the adsorption of a nanocluster at the rutile surface will prevent aggregation of the nanoclusters to larger structures and isolated nanoclusters will be present at the surface. While TiO_2 nanocluster modification of rutile has not been presented experimentally, the work from Tada *et al.* modifying rutile and anatase with other metal oxide nanoclusters[30-33] is shown to involve isolated metal oxide nanoclusters that do not aggregate to form larger clusters or films, even during the sintering treatment. Finally, experiments have been performed on the re-oxidation of reduced titania, and as illustrated in ref. 68, stoichiometric (1x2) ad-strings would appear to require a particular size of ad-cluster to form, hinting that other cluster sizes will not be favourable for this process.

When comparing the four Ti_5O_{10}-TiO_2 configurations, in all cases the clusters bond to surface with the creation of new Ti-O bonds. Configurations I, III and IV create five new Ti-O bonds and their adsorption energies are in the same range around -3 eV, while configuration II has four bonds and the most favourable cluster adsorption energy. For this configuration, two Ti atoms from the cluster (Ti_c) bond to two bridging O atoms from the surface (O_s) with Ti_c-O_s distances of 2.08 Å and 1.99 Å. Two bonds come from the O atoms from the cluster (O_c) with two 5 fold Ti atoms from the surface (Ti_s), with Ti_s-O_c distances of 1.88 Å and 1.99 Å. Comparing the cluster shape after deposition there is a reduction in the number of terminal oxygen atoms from two in the bare cluster to one after deposition. Finally, in the most stable configuration, distortions to the cluster structures are smallest. In all configurations the Ti_c - O_s bonds have the distances are in the range of 1.90 Å to 2.28 Å-and Ti_s-O_c bonds have distances in the range from 1.89 Å to 2.17 Å.

Figure 3 (a) – (e) presents the atomic structures of the most stable Ti_5O_{10}, Ti_6O_{12}, Ti_8O_{16}, $Ti_{16}O_{32}$ and $Ti_{30}O_{60}$ clusters adsorbed on the TiO_2 rutile (110) surface. The adsorption energies of the clusters range from -2.72eV for Ti_6O_{12} cluster to -6.71eV for the $Ti_{30}O_{60}$ cluster and show a distinct effect due to cluster size. The clusters bond to the surface forming new bonds: Ti_6O_{12} creates four new bonds, Ti_8O_{16} has eleven bonds, $Ti_{16}O_{32}$ creates seven bonds and $Ti_{30}O_{60}$ has six new cluster-surface bonds. Table 1 presents the bond lengths for new Ti-O bonds between the cluster and surface. The smaller clusters namely: Ti_5O_{10} and Ti_6O_{12}, are characterized by Ti_c-O_s distances in the range from 1.92 Å to 2.08 Å. The bigger clusters, Ti_8O_{16}, $Ti_{16}O_{32}$ and $Ti_{30}O_{60}$, present Ti_c-O_s distances in the range 1.87 Å to 2.12Å.

For all clusters O_c-Ti_s distances are similar, ranging from 1.84 Å to 1.99 Å. In general the Ti-O distances involving the surface Ti interacting with cluster oxygen are shorter than in the Ti-O distances involving cluster Ti interacting with the surface oxygen. This occurs since the surface Ti atoms reach a 6-fold coordination environment upon binding to the cluster, but cluster Ti atoms are not always able to maximise interaction with the surface oxygen, so that longer Ti-O distances are obtained for some cluster Ti species. In the adsorbed Ti_6O_{12} cluster, the cluster Ti that bind to the surface oxygen are able to form Ti-O bonds with typical Ti-O bond distance and achieve 6-fold coordination. In other clusters, some cluster Ti species can bind in this way, but the clusters are unable to relax their structure to allow all Ti atoms find 6-fold coordination.

Comparing the geometries of the bare and deposited clusters there is generally not a big change in terms of Ti-O bond distances and the number of terminal oxygen atoms stays the same. A different situation is found for the Ti_8O_{16} cluster where there is a big change in the geometry of the deposited cluster and the number of terminal oxygen atoms is reduced from three in the bare cluster to zero in deposited one. $Ti_{16}O_{32}$ has an unchanged number of terminal oxygen atoms after relaxation. The adsorbed $Ti_{30}O_{60}$ cluster results in small changes to the geometry, as a result of cluster-surface interfacial bonding, and a reduction in the number of terminal oxygen atoms from eight in bare cluster to four. It is important to point out that the cluster with the least negative adsorption energy has no change in the number of terminal oxygen atoms while in other clusters, with more favourable adsorption energies, there is always a reduction in the number of terminal oxygen atoms, so that increasing the coordination of terminal oxygen atoms may play an important role in the stability of adsorbed clusters at the TiO_2 surface.

Table 1: Surface – cluster Ti-O distances, in Å, for: Ti_5O_{10}, Ti_6O_{12}, Ti_8O_{16}, $Ti_{16}O_{32}$, $Ti_{30}O_{60}$ clusters on TiO_2 rutile (110) surface. Ti^c and O^c signify Ti and O from the TiO_2 cluster and Ti^s and O^s signify Ti and O from the surface. Also included are Ti-O distances in bulk rutile TiO_2

Structure	Ti^c-O^s	Ti^s-O^c
Ti_5O_{10}	2.08	1.99
	1.99	1.88
Ti_6O_{12}	1.92	1.94
	1.92	1.91
Ti_8O_{16}	1.90	1.87
	2.09	1.96
	2.08	1.91
	1.95	1.87
	1.97	2.09
	2.11	
$Ti_{16}O_{32}$	2.12	1.98
	2.00	1.85
	2.06	1.90
	2.08	
$Ti_{30}O_{60}$	2.11	1.90
	2.18	1.84
	2.05	
	2.03	
Bulk Rutile	1.96, 2.00	

A final point is that of the terminal, titanyl, oxygens that are found in the anchored TiO_2 nanocluster on many of our heterostructures and the question of their stability, given the expected reactivity of such species. In the literature, one can find some examples of titanyl species [62-65, 69-74], including in free TiO_2 nanoclusters[62-65] (which are also found in this work) and proposed in the rutile (011) (2x1) reconstructed surface[70-73]. Given that the free nanoclusters are stable with titanyl groups, it is not so surprising that the majority of the adsorbed cluster structures are also stable with titanyl groups and these are found in both the QEq and DFT+U relaxations. Examining the impact of annealing and processing over time and any change to the titanyl species will require dynamics simulations, but in addition, experimental synthesis and characterisation of these structures would also shed important information on the formation and stability of the titanyl species found in these simulations.

A final important point to consider is that of the possibility of water adsorption, in particular given the terminal oxygens present in the adsorbed nanoclusters. The structures studied in this paper could be potentially useful for photocatalytic water splitting to hydrogen. This process would involve adsorption of water at the nanocluster, adsorbing most likely at undercoordinated Ti sites and likely dissociating into H and OH, with adsorption of H at the titanyl oxygen atoms[65], which may be important for realistic photocatalytic activity. While this is an important issue to examine, it requires a detailed modelling and experimental treatment, and therefore lies beyond the scope of this paper, which is to examine the basic properties of potential photocatalysts, but this is work that is being undertaken.

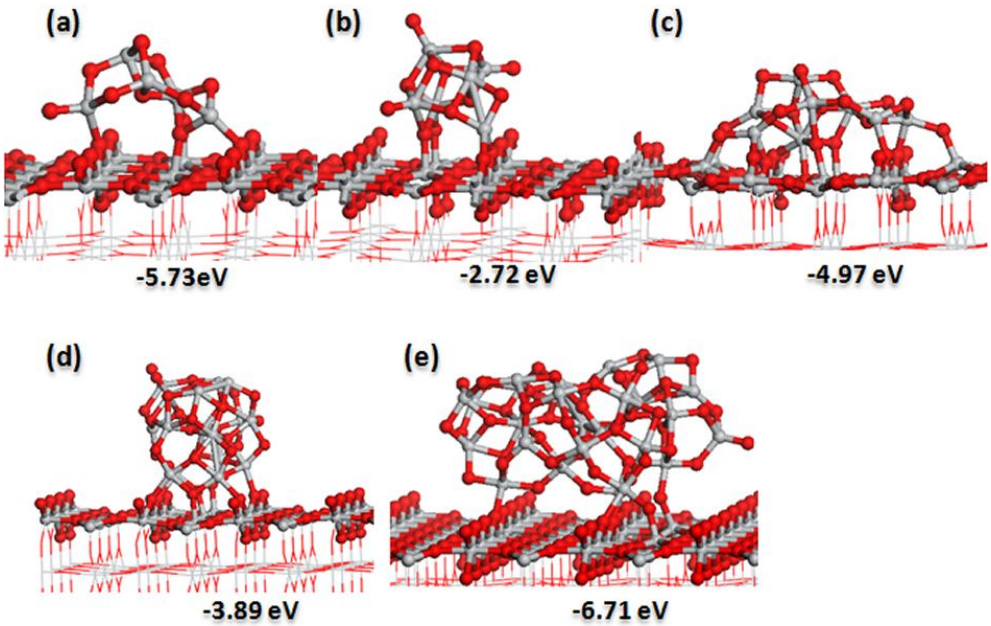


Fig. 3 Atomic structures and adsorption energies (in eV) of most stable (a) Ti_5O_{10}, (b) Ti_6O_{12}, (c) Ti_8O_{16}, (d) $Ti_{16}O_{32}$, (e) $Ti_{30}O_{60}$ clusters adsorbed on TiO_2 rutile (110) surface. The colour scheme is the same as figure 1.

To study the effect of modifying the rutile (110) surface with the TiO_2 clusters on the electronic structure, figure 4 presents the projected electronic density of states (PEDOS), projected onto the Ti 3d and O 2p states of the cluster and the surface, which allows us to examine the relative positions of the cluster and surface derived electronic states around the band gap and determine the effect of cluster deposition on the band gap of TiO_2.

The PEDOS firstly indicates that there are no defect states in the band gap, which would arise from formation of reduced Ti^{3+} species after cluster deposition and relaxation. To further confirm this, the computed the Bader charges for Ti and O

ions in the (110) surface and the supported clusters are shown in table 2, where we have grouped the oxygen into 1, 2, or 3-fold coordinated. In the (110) surface, we compute Ti charges of around 1.4e$^-$, typical of Ti^{4+} in TiO_2, while in the deposited clusters, the Bader charges are as follows: in Ti_5O_{10} the Ti charge is 1.33 - 1.38e$^-$, in Ti_6O_{12} the Ti charge is 1.35 - 1.45e$^-$, in Ti_8O_{16} the Ti charge is 1.33 - 1.39e$^-$, in $Ti_{16}O_{32}$, the Ti charge is 1.27 - 1.39e$^-$ and in $Ti_{30}O_{60}$ the Ti charge is 1.28 - 1.41e$^-$. Thus, the clusters also have exclusively Ti^{4+} ions.

The oxygen charges show the most interesting effects due to formation of the heterostructures. Firstly, the Ti_8O_{16}-TiO_2 structure is found to have no terminal oxygen atoms and the Bader charges for oxygen in the cluster also show that there are no terminal oxygen atoms upon formation of the heterostructure. Instead, only 2 and 3-fold coordinated oxygen are present, with the Bader charge being modified to one consistent with 2 or 3 coordinated oxygen.

For the other TiO_2 nanoclusters, we find that the terminal oxygens have Bader charges that are similar to those computed for terminal oxygen in the free nanoclusters, thus also confirming the presence of these oxygen. For Ti_5O_{10}, one previously terminal oxygen is now 2-fold coordinated by binding to a surface Ti atom and the computer Bader charge reflects this, being 7.27 electrons. The computed Bader charges for oxygen in ther other nanoclusters also show a similar change in the oxygen coordination.

Table 2: Computed Bader Charges for Ti and O in the heterostructures. The O charges are divided into different groups depending on O coordination.

Structure	Q^{Ti}	Q^{O1fold}	Q^{O2fold}	Q^{O3fold}
Ti_5O_{10}	1.35; 1.38; 1.39; 1.33; 1.37;	7.14	7.3; 7.27	7.4; 7.34
Ti_6O_{12}	1.45: 1.45; 1.38; 1.35; 1.42	7.11; 7.17; 7.12	7.29 7.3	7.38; 7.37; 7.35; 7.39
Ti_8O_{16}	1.34; 1.33; 1.39; 1.33; 1.35;	--	7.31 7.28; 7.26; 7.33	7.32 7.39
$Ti_{16}O_{32}$	1.37; 1.34; 1.27; 1.30; 1.38; 1.34; 1.32; 1.36; 1.37; 1.34; 1.35; 1.40;	7.11	7.31 7.28 7.29; 7.26; 7.27: 7.28	7.37 7.38; 7.4; 7.37; 7.41; 7.34; 7.38; 7.35
$Ti_{30}O_{60}$		7.13	7.27 7.28; 7.26; 7.31; 7.27; 7.3;	7.38; 7.35; 7.37; 7.38; 7.39; 7.42
Bulk Rutile	1.40			7.70

We are interested in determining the effect of nanocluster surface modification on the energy gap of TiO_2 and any changes to the composition of the valence (VB) and conduction bands (CB) as a result of interface formation between the surface and the clusters. In all cases, except for Ti_8O_{16}, the PEDOS shows, as a result of the formation of interfacial Ti-O bonds, that the top of the VB now predominantly comes from TiO_2 cluster electronic states, with the surface dominated VB states liying at lower energy. We find, upon examination of the cluster O 2p DOS, that the terminal oxygen atoms on the clusters dominate the top of the cluster-derived VB states (supporting information, figure S3, in which the PEDOS for terminal cluster oxygen and non-terminal cluster oxygen are shown). As a consequence of the cluster-surface interaction, the VB edge is shifted to higher energy compared to the bare surface, with the magnitude of the shift depending on the size of the cluster. At the same time, the bottom of the conduction band is made up of contributions from surface Ti 3d states, with the cluster derived states generally lying higher in energy; for the larger clusters this is around 0.2 eV above the CB edge. We therefore propose that the shift in the position of the VB edge upon adsorption of TiO_2 cluster will lead to a reduction in the energy gap relative to bare TiO_2, consistent with our previous results for smaller TiO_2 clusters[35] and FeO_x deposited on rutile (110)[34], as well as experimental results on FeO_x and NiO clusters deposited on TiO_2[29-31]. Table 3 presents the simple valence conduction band energy gaps for each heterostructure, as well as the bare rutile (110) surface.

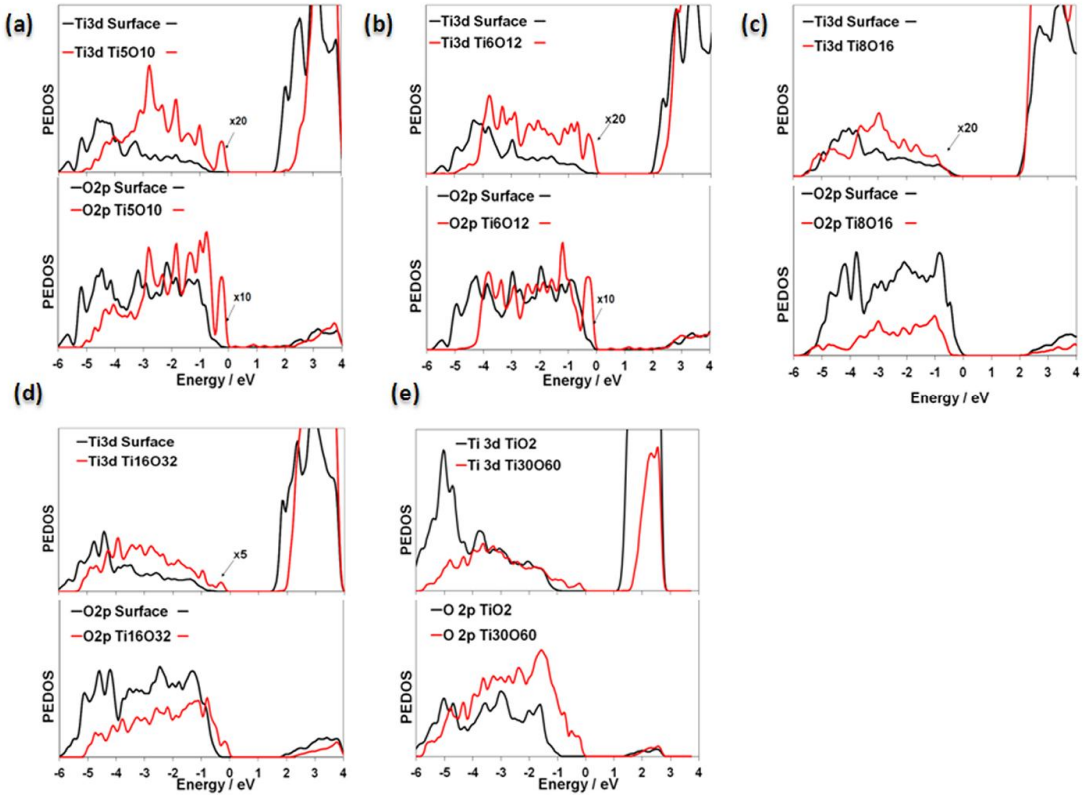


Fig. 4 Electronic density of states projected (PEDOS) onto surface (black line) and nanocluster (red line) Ti 3d and O 2p states for (a) Ti_5O_{10}, (b) Ti_6O_{12}, (c) Ti_8O_{16}, (d) $Ti_{16}O_{32}$, (e) $Ti_{30}O_{60}$ clusters supported on TiO_2 rutile 110 surface. O 2p PEDOS for different oxygen atoms in the nanoclusters are shown in the supporting information as described in the text. For some structures, the cluster PEDOS is multiplied by the amount indicated in order to enhance its visibility relative to the surface. The zero of energy is the top of the occupied states.

The Ti_8O_{16} cluster is the only deposited cluster that gives no states in the band gap of the TiO_2 surface and therefore leads to no change in the energy gap relative to the bare surface. One of the reasons for this may be that there is a substantial change in the geometry of cluster Ti_8O_{16} after deposition when compared to other clusters, including the loss of the terminal oxygen atom. This results in a structure in the cluster that is more consistent with bulk TiO_2, with Ti-O distances in the cluster 1.85Å - 2.11Å. In addition, this may be a cluster that has an energy level alignment with the surface such that upon formation of the interface, the cluster and surface VB and CB edges coincide.

Table 3: Computed energy gaps (the energy difference between valence and conduction band edges) and the optical gaps (from Tauc plots, see text) of the heterostructures from DFT+U.

Heterostructure	Energy Gap / eV	Optical Gap / eV
Rutile (110)	2.1	1.70
Ti_5O_{10}-TiO_2	1.6	1.55
Ti_6O_{12}-TiO_2	1.55	1.55
Ti_8O_{16}-TiO_2	2.1	1.65
$Ti_{16}O_{32}$-TiO_2	1.4	1.60
$Ti_{30}O_{60}$-TiO_2	1.1	1.45

The computed values of the simple valence-conduction band energy gap is given in table 3 for the unmodified rutile(110) surface and the nanocluster modified surface, showing (with the exception of Ti_8O_{16}) a reduction in the energy gap with surface modification. This reduction arises from the presence of the electronic states from the deposited cluster, which shifts the valence band to higher energy, means that we predict that these hetereostructures will have improved photocatalytic activity, at least in terms of light absorption in the visible region of the solar spectrum. There are no obvious trends in the computed DFT+U energy gaps with the size of the nanocluster, which would be expected for nanoclusters of TiO_2 of this size[62-65].

The shifts in the energy gaps determined from the DOS analysis are from simple Kohn-Sham energy eigenvalue differences, which do not have the same physical meaning as an excitation energy. Therefore, care needs to be taken in making predictions of shifts in the energy gaps as a result of modifying TiO_2 with the nanocluster. To confirm the effect of surface modification on the light absorption properties of rutile (110), we have also computed the optical (Tauc) gap of the heterostructures. Figure 5 and (figure S4 of the supporting information) show the plots of absorption coefficient versus energy for the bare rutile surface and the heterostructures. We see that the optical gap changes with surface modification of rutile with the TiO_2 nanoclusters, which is consistent with the overall finding of the DOS analysis. With the largest $Ti_{30}O_{60}$ nanocluster, a reduction in the optical gap of 0.25 eV indicates the potential to shift light absorption into the visible region. We also generally see a smaller absorption coefficient

for surface modified TiO_2, consistent with localised O 2p states at VB top which would be expected to show a smaller transition matrix element compared to the bare surface, which itself has localised O 2p states at the top of the VB arising from the bridging oxygen atoms in the surface.

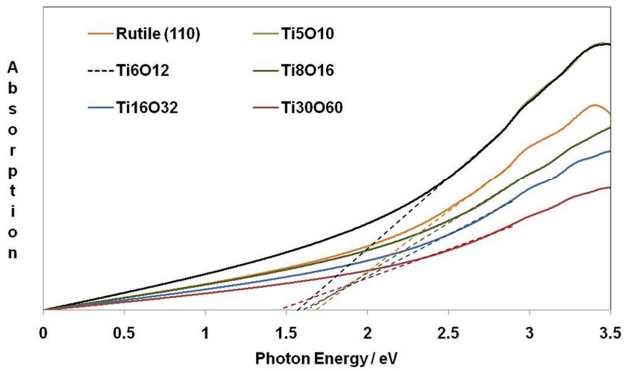


Fig. 5 Computed optical absorption spectrum (Tauc plot) for unmodified rutile (110) and TiO_2 nanocluster modified rutile (110). See figure S5 for a close-up view of the linear extrapolation in determining the optical gap.

Since the top of the VB is (with the exception of the Ti_8O_{16} cluster) dominated by electronic states from the adsorbed TiO_2 cluster and particularly the terminal oxygen atoms, it is reasonable to expect that the separation of electrons and holes will be improved over bare TiO_2. Di Valentin and Selloni[75] and Jededi *et al.*[76] have shown in a model of the triplet excited state of bulk TiO_2 that upon excitation, a Ti^{3+} and an oxygen hole (O^-) are formed after an electron is excited from the VB to the CB. Similarly, in the present heterostructures the composition of the VB (from the cluster) and CB (from the surface) will result in holes being found on oxygen of the cluster and electrons on Ti atoms of the surface, that is the electron and hole will be spatially separated. In fact, upon examination of the DOS at the VB edge, we suggest that the terminal oxygen atoms in the supported cluster will be likely sites for trapping the hole formed after excitation, while electrons will be trapped at surface Ti atoms; a detailed analysis of this point is beyond the scope of this paper and further work is in progress to examine models of this excited state. This is important for photocatalysis, since charge separation generally leads to longer charge carrier lifetimes and reduced charge recombination so that photocatalytic activity will be improved compared to pure TiO_2. PL spectroscopy is used as a probe of charge recombination, with particular peaks observed for TiO_2 arising from the recombination of electrons and holes[77]; the work of Tada et al. shows a diminution of the TiO_2 PL peak at 540 nm for FeO_x modified TiO_2[30-33].

Table 4: Computed workfunction of the bare rutile (110) TiO_2 surface and the $(TiO_2)_n$-TiO_2 heterostructures from DFT+U.

Heterostructure	Workfunction / eV
TiO_2 (110)	7.10 eV
Ti_5O_{10}-TiO_2	6.83 eV
Ti_6O_{12}-TiO_2	6.89 eV
Ti_8O_{16}-TiO_2	6.50 eV
$Ti_{16}O_{32}$-TiO_2	5.28 eV
$Ti_{30}O_{60}$-TiO_2	6.25 eV

We have computed the workfunction of the heterostructures and compared this to the unmodified rutile (110) surface. The workfunction is calculated as the difference between the Fermi energy of the surface and the vacuum energy and is shown for each case in table 4. Compared to the bare (110) surface, while all heterostructures show a reduction in the workfunction this change depends on the exact cluster size. A workfunction reduction is of benefit as it facilitates a reduction in the barrier for electron transfer to an adsorbed species, e.g. gold, which could be important for applications in catalysis using metal oxide heterostructures.

Finally, to determine if the results presented above are significantly affected by the use of DFT+U compared to DFT, figure 6 presents a comparison of the PEDOS for the Ti_5O_{10}-TiO_2 heterostructure, for surface TiO_2 (110) Ti 3d states and adsorbed cluster states from DFT and DFT+U. The energy gap from DFT for pure rutile (110) is strongly underestimated at around 1.8eV, but upon examination of the PEDOS plots we find that the general description of the electronic states is the same as DFT+U, namely that the top of VB is from the cluster and the CB comes from the surface with a band gap reduction.

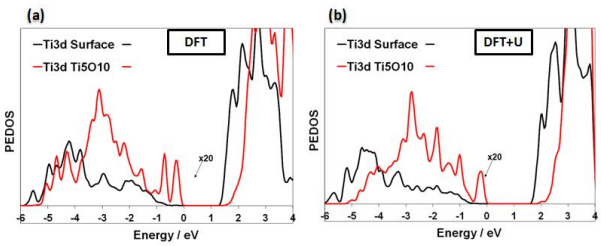


Fig.6 Comparison of electronic density of states projected (PEDOS) on Ti 3d states for TiO_2 rutile (110) surface and adsorbed Ti_5O_{10} cluster (a) DFT results, (b) DFT+U results.

4 Discussion

In this work, we have examined surface modification of rutile TiO_2 by TiO_2 nanoclusters, with diameters up to 1.5 nm diameter; these clusters are at the size that can be achieved in experiments. The modification of the rutile surface and formation of strong interfacial Ti-O bonds between the cluster and the surface modifies the electronic structure, so that the valence band edge is pushed upwards in energy, thus lowering the energy gap compared to the bare surface; the precise shift of the VB edge depends on the cluster size, typical for such small metal oxide clusters. We suggest therefore that this surface modification could lead to an increase in visible light absorption compared to the unmodified surface.

While much focus has been on modifying TiO_2 to give visible light absorption, reducing the propensity for electrons and holes to undergo non-radiative recombination is important. In the present structures, the energy band alignments are such that the VB edge is dominated by oxygen states from the deposited cluster and the conduction band edge by Ti 3d states from the surface, so that upon excitation, electrons will be found on Ti in the rutile (110) surface and holes on the cluster, which will improve the activity since recombination of electrons and holes will now be reduced over the bare surface. The presence of one or more terminal oxygen atoms in the supported cluster provides potential hole trapping states after excitation. Recombination of the trapped hole with electrons will be diminished, facilitating the use of both charge carriers in oxidation and reduction reactions. The advantage of this for dye degradation has been discussed by Tada and co-workers[30-33]. We also find that the workfunction of the composite is reduced by around 1 eV compared to the bare surface, which will be important for enhanced reactivity.

The importance of forming an interface between two materials to enhance photocatalytic activity is discussed in the literature[23-41] and new materials combinations are being prepared, e.g. Ismail reported a synthesis of PdO-TiO_2 nanocomposite through one-step sol-gel reaction with enhanced photocatalytic activities[78]. The activity was tested by the determination of the rate of HCHO formation generated by the photooxidation of CH_3OH. While enhancement of photocatalytic activity was found only in the UV region, with no change in the TiO_2 band gap, achieving electron-hole separation was a key feature to enhance the photocatalytic activity. Tada at al showed that SnO_2 clusters dispersed on TiO_2 anatase will enhance UV activity (tested by photocatalytic decomposition of 2-naphthol) with improved hole/electron separation because, as shown by DFT calculations, the excited electrons will be found on the adsorbed SnO_2 species which act as mediator for the electron transfer to, e.g. O_2[32]. The importance of interface in the light absorption and photocatalytic activity of a heterostructure was pointed out by Kong at al where two semiconductors different in properties where combined to create photocatalyst with high photocatalytic activities under visible-light on degradation of Rhodamine B[24]; heterojunctions with a type II staggered band alignment can improve transfer of charge carriers and also reduce hole/electron recombination. The present simulations show that formation of the interface is key to modifying the electronic properties of photocatalytically active materials and future work will focus on deepening our understanding of the key factors determining the activity of metal oxide heterostructures.

5. Conclusions

We have presented DFT+U simulations of the properties of nanoclusters of $(TiO_2)_n$ (n=5, 6, 8, 16, 30) deposited on the TiO_2 rutile (110) surface which form a novel heterostructure that can function as a visible light active photocatalyst. These heterostructures show the following important results:

- The TiO_2 nanoclusters adsorb strongly on the rutile (110) surface, with adsorption energies in the range of -2.7eV to -6.7eV and forming new interfacial Ti-O bonds and the clusters are thermodynamically stable towards aggregation to larger clusters or films.
- The electronic structure indicates a (nanocluster dependent) reduction in the band gap in the heterostructure compared to the unmodified surface. While the present results indicate the possibility of visible light absorption, experimental confirmation of this conclusion would be welcome.
- The valence band edge is derived from the cluster electronic states and the conduction band edge is composed of surface states. Upon photoexcitation this will facilitate spatial separation of electrons and holes, thus reducing charge recombination. This in turn leads to improved photocatalytic activity.
- A reduction in the workfunction compared to the bare surface can be achieved, which is useful for reactivity in catalysis.

These features of these novel heterostructured materials make them promising for visible light active photocatalysis.

Acknowledgements

AI and MN acknowledge support from Science Foundation Ireland (SFI) through the Starting Investigator Research Grant Program "EMOIN" project, grant number SFI 09/SIRG/I1620. PAM acknowledges support from EPSRC grant EP/C524349. We acknowledge the support of the European Union through the Cost Action CM1104 "Reducible oxide chemistry, structure and functions". We acknowledge computing resources at Tyndall provided by SFI and by the SFI and Higher Education Authority funded Irish Centre for High End Computing.

Notes and references

[a] *Tyndall National Institute, University College Cork, Lee Maltings, Cork, Ireland*
[b] *Department of Chemical Engineering, University of Strathclyde, Glasgow G1 1XQ, Scotland, UK*
E-mail: michael.nolan@tyndall.ie

†Electronic Supplementary Information (ESI) available: Figure S1 and S2: high energy cluster adsorption structures at the rutile (110) surface. Figure S3: PEDOS for terminal and non-terminal TiO_2 nanocluster oxygen. See DOI: 10.1039//

1. H. Yu, H. Irie, Y. Shimodaira, Y. Hosogi, Y. Kuroda, M. Miyauchi, and K. Hashimoto, *J. Phys. Chem. C*, 2010, **114**, 16481
2. N. Murakami, T. Chiyoya, T. Tsubota and T. Ohno, *Appl. Catal. A*, 2008, **348**, 148
3. K-J Shieh, M. Li, Y-H. Lee, S-D. Sheu, Y-T. Liu and Y-C. Wang, *Nanomedicine: Nanotechnology, Biology and Medicine,* 2006, **2,** 121
4. C. W. Dunnill, K. Page, Z. A. Aiken, S. Noimark, G. Hyett, A. Kafizas, J. Pratten, M. Wilson, and I. P. Parkin, *J. Photochem and Photbiol A* , 2011, **220**, 113
5. M. Ni, M. Leung, D. Leung and K. Sumathy, *Renew. Sust. Energ. Rev.* 2007, **11**, 401
6. A. Fujishima, X. Zhang and D. A. Tryk, *Surf. Sci. Rep.* 2008, **63**, 515
7. J. Nowotny, *Energy Environ. Sci.* 2008, **2**, 656
8. A. Fujishima, T. N. Rao and D. A. Tryk, *J. Photochem. And Photobiol. C,* 2000, **1**, 1.

9. L. Peng, T. Xie, Y. Lu, H. Fan and D. Wang, *Phys. Chem. Chem. Phys*., 2010, **12**, 8033
10. C. Di Valentin, G. Pacchioni, H. Onishi, and A. Kudo, *Chem. Phys. Lett.,* 2009, **469**, 166
11. C. Di Valentin, E. Finazzi, G. Pacchioni, A. Selloni, S. Livarghi, M. C. Paganini and E. Giamello, *Chem. Phys*., 2007, **339**, 44
12. J. G. Yu, Q. J. Xiang, M. H. Zhou and X. Y. Zhou, *Appl Cat. B Environmental*, 2009, **90**, 595
13. R. Long and N. J. English, *J. Phys. Chem. C,* 2010, **114**, 11984
14. J. W. Zheng, A. Bhattcahrayya, P. Wu, Z. Chen, J. Highfield, Z. L. Dong, and R. Xu, *J. Phys. Chem. C,* 2010, **114**, 7063
15. X. L. Nie, S. P. Zhou, G. Maeng, and K. Sohlberg, *Int. J. Photoenergy* 2009, article 294042
16. Y. Cui, H. Du, and L. S. Wen, *J. Mat. Sci. and Tech.* 2008**, 24**, 675
17. H. W. Peng, J. B. Li, S. S. Li and J. B. Xia, *J. Phys.: Condes. Matt.* 2008, **20**, 125207
18. L. Bian, M. X. Song, T. L. Zhou, X. Y. Zhao and Q. Q. Dai, *J. Rare Earths* 2009, **27**, 461
19. Y. Q. Gai, J. B. Li, S. S. Li, J. B. Xia and S. H. Wei, *Phys. Rev. Lett.* 2009, **102**, 036402
20. W. G. Zhu, X. F. Qiu, V. Iancu, X. Q. Chen, H. Pan, W. Wang, N. M. Dimitrijevic, T. Rajh, H. M. Meyer, M. P. Paranthaman, G. M. Stocks, H. H. Weitering, B. H. Gu, G. Eres and Z. Y. Zhang, *Phys. Rev. Lett*. 2009, **103**, 2264101
21. J. Zhang, C. X. Pan, P. F. Fang, J. H. Wie and R. Xiong, *ACS Applied Materials and Interfaces,* 2010, **2,** 1173
22. A. Kubacka, M. Fernandez-Garcia and G. Colon, *Chem. Rev*. 2012, **112***,* 1555
23. Y. Cao, T. He, Y. Chen, and Y. Cao, *J. Phys. Chem C*, 2010, **114**, 3627
24. L. Kong, Z. Jiang, T. Xiao, L. Lu, M. Jones, and P. P. Edwards, *Chem. Commun.,* 2011, **47**, 5512
25. H. Cheng, B. Huang, Y. Dai, X. Qin and X. Zhang, *Langmuir,* 2010, **26**, 6618
26. S. Hong, S. Lee, J. Jang and J. Lee, *Energy Environ. Sci*., 2011, **4**, 1781
27. T. Cao, Y. Li, C. Wang, Z. Zhang, M. Zhang, C. Shao and Y. Liu, *J. Mater. Chem*., 2011, **21**, 6922
28. V. Bharat, R. Boppana, and R. F. Lobo, *ACS Catal.,* 2011, **1**, 923
29. J. Libera, J. Elam, N. Sather, T. Rajh, and N. M. Dimitrijevic, *Chem. Mater.,* 2010, **22**, 409
30. (a) H. Tada, Q. Jin, H. Nishijima, H. Yamamoto, M. Fujishima, S-i. Okuoka, T. Hattori, Y. Sumida, and H. Kobayashi, *Angew. Chem. Int. Ed*. 2011, **50**, 3501. (b) Q. Jin, M. Fujishima, and H. Tada, *J. Phys. Chem C*, 2011, **115**, 6478
31. Q. Jin, T. Ikeda, M. Fujishima, and H. Tada, *Chem. Commun*., 2011, **47**, 8814
32. M. Fujishima, Q. Jin, H. Yamamoto, H. Tada, and M. Nolan, *Phys. Chem. Chem. Phys.,* 2012, **14**, 705
33. Q. Jin, M. Fujishima, M. Nolan, A. Iwaszuk and H. Tada*, J. Phys. Chem. C,* 2012, **116***,* 12631
34. M. Nolan*, Phys. Chem. Chem. Phys.*, 2011, **13**, 18194
35. A. Iwaszuk and M. Nolan, *Phys. Chem. Chem. Phys.,* 2011, **13**, 4963
36. M. Nolan, *Chem. Commun,* 2011, **47**, 8617
37. R. I. Bickley T. Gonzalez-Carreno, J. S. Lees, L. Palmisano and R. J. D. Tilley., *J. Solid St. Chem.* 1991, **92**, 178
38. G. Li and K. A. Gray, *Chem. Phys.*, 2007, **339***,* 173
39. G. Li, L. Chen, M. E. Graham, and K. A. Gray, *J. Mol. Catal. A*: *Chemical*, 2007, **275**, 30
40. G. Marcí, V. Augugliaro, M. J. López-Muñoz, C. Martín, L. Palmisano, V. Rives, M. Schiavello, R. J. D. Tilley and A. M. Venezia, *J. Phys. Chem. B* 2001, **105**, 1033
41. C. Karunakaran, R. Dhanalakshmi, P. Gomathisankar, and G. Manikandan, *J. Hazard. Mater*. 2010, **176**, 799
42. G. Kresse and J. Hafner, *Phys. Rev. B*, 1994, **49**, 1425.
43. P. E. Blöchl, *Phys. Rev. B,* 1994, **50**, 17953.
44. A. Iwaszuk and M. Nolan, *J. Phys. Chem. C*, 2011, **115**, 12995
45. J. P. Perdew, in Electronic Structure of Solids '91, ed. P. Ziesche and H. Eschrig, Akademie Verlag, Berlin, 1991.
46. V. I. Anisimov, J. Zaanen and O. K. Andersen, *Phys. Rev. B,* 1991, **44**, 943.
47. S. L. Dudarev, G. A. Botton, S. Y. Savrasov, C. J. Humphreys and A. P. Sutton, *Phys. Rev. B,* 1998, **57**, 1505.
48. B. J. Morgan, and G. W. Watson, *Surf. Sci*., 2007, **601**, 5034
49. M. V. Ganduglia-Pirovano, A. Hofmann, and J. Sauer, *Surf. Sci. Rep*. 2007, **62**, 219
50. M. Nolan, s. Grigoleit, D. C. Sayle, S. C. Parker, and G. W. Watson, *Surf. Sci.* 2005, **576**, 217
51. C. Di Valentin, G. Pacchioni and A. Selloni,.*Phys. Rev. B* 2004, **70**, 085116
52. A. M. Márquez, J. J. Plata, Y. Ortega J. F. Sanz, G. Colón ,A. Kubacka and M. Fernández-García, *J Phys. Chem. C*, 2012, **116**, 18759
53. http://www.freeware.vasp.de/VASP/optics
54. A. K. Rappe and W. A. Goddard III, *J. Phys. Chem*., 1991, **95**, 3358
55. W. Mortier, in *Structure and Bonding,* Kali S.; Jorgensen, C., Eds.; Springer: Germany, **1987**, vol. 66, p 125
56. P. A. Mulheran, M. Nolan, C. S. Browne, M. Basham, E. Sanville and R. A. Bennett, *Phys. Chem. Chem. Phys.,* 2010, **12***,* 9763
57. V. Swamy J. D. Gale, *Phys. Rev. B* **2000,** *62*, 5406
58. V. Swamy, J. D. Gale and L. S. Dubrovinsky, *Journal Phys. Chem. of Solids,* 2001, **62**, 88
59. A. Hallil, R. Te´tot, F. Berthier, I. Braems and J. Creuze, *Phys. Rev. B,* 2006, **73**, 165406
60. A. Hallil, E. Amzallag, S. Landron, and R. Tétot, *Surf. Sci,* 2011, **605***,* 738
61. D. J. Earl and M. W. Deem, *Phys. Chem. Chem. Phys.,* 2005, **7**, 3910
62. M. Calatayud and C. Minot, *J. Phys. Chem.* C 2009, **113,** 12186
63. S. A. Shevlin and S. M. Woodley, *J. Phys. Chem. C* 2010, **114,** 17333
64. S. Hamad, C. R. A. Catlow, S. M. Woodley, S. Lago and J. A. Mejias, *J. Phys. Chem. B* 2005, **109**, 15741
65. O. A. Syzgantseva, P. Gonzalez-Navarrete, M. Calatayud, S. Bromley and C. Minot. *J. Phys. Chem. C*, 2011, **115,** 15890
66. C. Loschen,A. Migani, S. T. Bromley, F. Illas and K. M. Neyman, *Phys. Chem. Chem. Phys.,* 2008, **10**, 5730
67. G. Henkelman, A. Arnaldsson and H. Jónsson, *Comput. Mater. Sci.,* 2006, **36**, 25
68. R. D. Smith, R. A. Bennett and M. Bowker, *Phys. Rev. B* 2002, **66**, 03540.
69. V. M. Bermudez, *J. Phys. Chem. C*, 2011, **115**, 6741
70. C. Di Valentin, A. Tilocca, A. Selloni, T. J. Beck, A. Klust, M. Batzill, Y. Losovyj and U. Diebold, *J. Am. Chem. Soc.* 2005, **127**, 9895
71. T. J. Beck, A. Klust, M. Batzill, U. Diebold, C. Di Valentin and A. Selloni, *Phys. Rev. Lett.* 2004, **93**, 036104.
72. X-Q. Gong, N. Khorshidi, A. Stierle, V. Vonk, C. Ellinger, H. Dosch, H. Cheng, A. Selloni, Y. He, O. Dulub and U. Diebold, *Surf. Sci.*, 2008, **603**, 138
73. H. Takahashi, R. Watanabe, Y. Miyauchi and G. Mizutani, *J. Chem. Phys.,* 2011, **134,** 154704
74. T. Rajh, J. M. Nedeljkovic, L. X. Chen, O. Poluektov and M. C. Thurnauer, *J. Phys. Chem. B* 1999, **103**, 3515
75. C. Di Valentin and A. Selloni, *J. Phys. Chem.. Lett.,* 2011**, 2**, 222
76. A. Jedidi, A. Markovits, C. Minot, S. Bouzriba and M. Abderraba, *Langmuir,* 2010, **26**, 16232
77. C. C. Mercado, F. J. Knorr, J. L. McHale, S. M. Usman, A. S. Ichimura, and L. V. Saraf, *J. Phys. Chem. C*, 2012**, 116***,* 10796
78. A. Ismail, *Appl. Catal. B: Environ.,* 2012, **117-118***,* 49

Graphical Abstract

Heterostructured photocatalysts: $(TiO_2)_n$ nanoclusters supported on TiO_2 rutile (110) are potential photocatalysts with visible light activity.

